ACCEPTED MANUSCRIPT

This is the author's peer reviewed, accepted manuscript. However, the online version of record will be different from this version once it has been copyedited and typeset.
PLEASE CITE THIS ARTICLE AS DOI:10.1063/5.0073692

AIP Advances

Temperature dependence of cathodoluminescence emission in irradiated Si-doped β-Ga_2O_3

Sushrut Modak [a)], Leonid Chernyak [a,g)], Alfons Schulte[a)], Minghan Xian [b)], Fan Ren [b)],

Stephen J. Pearton [c)], Arie Ruzin [d)], Sergey S. Kosolobov[e)],

Vladimir P. Drachev [e,f)]

[a] *Department of Physics, University of Central Florida, Orlando, FL 32816, USA*

[b] *Department of Chemical Engineering, University of Florida, Gainesville, FL 32611, USA*

[c] *Material Science and Engineering, University of Florida, Gainesville, FL 32611, USA*

[d] *School of Electrical Engineering, Tel Aviv University, Tel Aviv 69978, Israel*

[e] *Skolkovo Inst Sci & Technol, Ctr Design, Manufacturing & Mat, Nobel St, Bldg 1, Moscow 121205, Russia*

[f] *Univ North Texas, Dept Phys, Denton, TX 76203 USA*

Temperature dependent continuous and time-resolved cathodoluminescence measurements were employed to understand the luminescence from Si-doped β-Ga_2O_3 prior to irradiation and after 10 MeV proton and 18 MeV alpha-particle irradiation. The shape and location of the luminescence components (UVL' at 3.63 eV, UVL at 3.3 eV and BL at 2.96 eV) obtained from Gaussian decomposition did not change in either width or peak location, indicating that new radiation-induced trap-levels were non-radiative in nature between 4.5 K to 310 K temperature range. Activation energies, associated with thermal quenching of UVL' and UVL bands, show temperature dependence suggesting ionization of shallow Si-donors and a thermally-activated non-radiative process.

[g)] email: chernyak@physics.ucf.edu

ACCEPTED MANUSCRIPT

This is the author's peer reviewed, accepted manuscript. However, the online version of record will be different from this version once it has been copyedited and typeset.
PLEASE CITE THIS ARTICLE AS DOI:10.1063/5.0073692

AIP Advances

In recent years, β-Ga_2O_3 has attracted interest due to its wide-bandgap (~4.5-4.9 eV) and high critical field strength (~ 8 $MVcm^{-1}$). These properties enable a unique set of applications involving high power electronics, such as high frequency, low loss power switching, and true UV-blind photodetection [1-11]. With a high atomic displacement energy and wide bandgap, β-Ga_2O_3 is also a robust material, suitable for applications involving extreme temperature and radiation, such as electronics deployed in low earth satellite orbits [1, 12], where devices must withstand fluxes of high energy particles emitted from solar flares.

The study of intrinsic and radiation-induced defects is challenging in β-Ga_2O_3 due its complex structure. β-Ga_2O_3 has a monoclinic structure with two crystallographically different Ga positions - a tetrahedral Ga(I) and an octahedral Ga(II); Oxygen is trigonally (O(I), O(II)) and tetrahedrally O(III) coordinated [13, 14]. The nature of defects varies based on the method of irradiation and the primary defects can potentially recombine to form complexes. To investigate this further, several studies have been performed to explore the detrimental effects of high energy radiation on formation of various defects and their effect on carrier transport properties in β-Ga_2O_3 [15-25]. The current study described here was conducted to understand the temperature-dependent luminescence behavior of defects, generated by proton and alpha particles, in Si-doped β-Ga_2O_3 with continuous and time-resolved cathodoluminescence (CL) measurements.

The samples under test consisted of 20 µm thick epitaxial β-Ga_2O_3 layers deposited by Halide Vapor Phase Epitaxy (HVPE) on Sn-doped n^+-β-Ga_2O_3 substrate grown with Edge-defined Film-fed Growth (EFG) technique. The substrate was oriented in [001] direction with carrier concentration of ~ 2.2×10^{18} cm^{-3}. The epitaxial β-Ga_2O_3 layer was doped with Si (electron concentration of ~ 3.6×10^{16} cm^{-3}, obtained from room temperature Hall measurement) and planarized to a thickness of 10 µm with chemical/mechanical polishing. A part of the samples was

AIP Publishing

ACCEPTED MANUSCRIPT

This is the author's peer reviewed, accepted manuscript. However, the online version of record will be different from this version once it has been copyedited and typeset.
PLEASE CITE THIS ARTICLE AS DOI:10.1063/5.0073692

AIP Advances

exposed to 18 MeV alpha particle radiation (fluence of ~ $1x10^{12}$ cm^{-2}) and others were exposed to 10 MeV proton radiation with fluence of $5x10^{12}$ cm^{-2}. A set of samples were kept aside (reference) to take baseline measurements. The irradiation was performed at the MC-50 cyclotron at Korea Institute of Radiological and Medical Science. In both proton and alpha irradiation, the 10 µm-thick Si-doped β-Ga_2O_3 layer was completely irradiated with penetration depth of 330 µm and 80 µm, respectively. Carrier removal rates in both cases were found to be 237 cm^{-1} and 406 cm^{-1}. More details on the fabrication procedure can be found elsewhere [19, 25].

Temperature-dependent cathodoluminescence was performed in the range from 4.5 to 310 K on Attolight Allalin 4027 Chronos Scanning Electron Microscope (SEM) fitted with a temperature-controlled stage (CryoVAC TIC 500). The electron beam accelerating voltage was kept fixed at 10 keV for all measurements. The CL emission was dispersed with a single grating with 150 grooves/mm blazed at 500 nm (Jobin-Vyon iHR320 spectrometer). The CL spectra were recorded with a CCD camera (Andor Newton 920P) sensitive between 180-1100 nm. Electron pulses (~ 8 ps width) for time-resolved cathodoluminescence (TRCL) measurements were generated by illumination of the electron gun tip with a femtosecond laser (Onefive Genki HP-03, 80 MHz) after reducing the filament heating current to thermionic emission threshold from continuous mode operation. The TRCL signal emitted from the sample was recorded after grating dispersion on a streak camera (Optronis Optoscope, 2 ps resolution) synchronized with the laser. Additional details about the TRCL measurements can be found in ref. [17].

The photoluminescence (PL) and CL emission spectra of β-Ga_2O_3 reported in the literature do not exhibit radiative recombination in the vicinity of the bandgap (near band edge (NBE) emission) and instead, contain several broad emission bands [26-28]. Broad PL spectra with large Stokes shift and convergence of Urbach tails are an indicator of the self-localization of holes [29, 30].

AIP Publishing

ACCEPTED MANUSCRIPT

This is the author's peer reviewed, accepted manuscript. However, the online version of record will be different from this version once it has been copyedited and typeset.
PLEASE CITE THIS ARTICLE AS DOI:10.1063/5.0073692

AIP Advances

With the help of electron paramagnetic resonance (EPR) measurements, it was found that the self-trapped holes (STHs) in β-Ga2O3 are not stable above 110 K [31]. This was verified independently by measuring the diffusion length of holes in several Electron Beam-Induced Current (EBIC) studies of n-type β-Ga_2O_3 [17, 18, 24, 32-36]. However, the NBE emission remains absent for temperatures higher than 110 K, despite a significant portion of holes being mobile. In contrast, NBE was observed at sufficiently high PL excitation energies [37], large enough to saturate the STHs, which have an estimated concentration of ~ 6.4×10^{19} cm^{-3} [38]. It can be speculated that the lifetime of STH is relatively short at higher temperatures, but self-trapping still occurs due to the low trapping barrier energy [29, 39], serving as an intermediary step before disassociation. The three commonly reported bands in the β-Ga_2O_3 emission are ultraviolet luminescence (UVL) in the range of 3.2-3.6 eV, blue-luminescence (BL) from 2.5-2.8 eV and green luminescence (GL) from 2.2-2.4 eV.

Fig. 1a shows the temperature dependence of measured raw CL spectrum from 4.5 K to 310 K for the reference sample. As seen in previous luminescence studies on β-Ga_2O_3, the CL signal is thermally quenched above 100 K [40-43]. Fig. 1b and 1c show Gaussian decompositions of the normalized CL emission spectra for the reference sample at 4.5 K and 310 K. The UVL and BL bands were found to be centered at 3.3 eV and 2.96 eV at 4.5 K respectively. An additional luminescence band UVL' at 3.63 eV was observed. UVL band exhibited the strongest emission in the entire temperature range of measurements (4.5 - 310 K). It can be seen from Figs. 1b and 1c, that the contribution of BL band to the total luminescence increases with increasing temperature, as opposed to UVL and UVL' bands.

UVL is associated with self-trapped excitons (STEs), consisting of a STH and a bound electron, due to the absence of NBE, independence of impurity doping, and a large Stokes shift in

AIP Publishing

ACCEPTED MANUSCRIPT

This is the author's peer reviewed, accepted manuscript. However, the online version of record will be different from this version once it has been copyedited and typeset.
PLEASE CITE THIS ARTICLE AS DOI:10.1063/5.0073692

AIP Advances

the photoluminescence spectrum of β-Ga_2O_3 [29-31, 38, 39, 44]. Broad STE emission width is associated with phonon coupling arising from the strong lattice distortion around the STH. STE emission is commonly observed in alkali halides [45]. Theoretical calculations indicate the tendency of holes in β-Ga_2O_3 to form small polarons (STHs) with lattice distortion, with two possible stable locations - O(I) and between two O(II). The O(I) and dual O(II) excitons differ in emission energies, which are found to be ~3.7 eV and 3.2-3.6 eV respectively [28, 46]. STEs are strongly coupled to the lattice, and the luminescence spectrum exhibit Gaussian broadening [41, 45]. UVL' and UVL were identified in the Gaussian decomposition of the luminescence spectra, as seen in Figs. 1b and 1c. The origin of these peaks is tentatively assigned to O(I) and dual O(II) sites, based on their peak location [40, 42, 46, 47]. The difference in the intensities of UVL' and UVL was attributed to two configuration groups, roughly present in the same ratio as that for their emission intensities [47]. Moreover, the sensitivity to PL excitation polarization of the two bands originates from the orientation of the STH. The PL polarization dependence was found to be slightly different for UVL' and UVL [47-50].

The BL emission arises from a donor-acceptor pair transition involving V_{Ga} acceptors or a (V_o-V_{Ga}) complex [43]. In intentionally n-doped β-Ga_2O_3, the formation energy of V_{Ga}^{-3} is much smaller than for the (V_o-V_{Ga}) complex [28] and is expected to become a majority hole-trap. The origin of the donor level was originally believed to be V_O due to the relation between resistivity, the formation energy of V_O, and their correlation with blue luminescence [42, 43]. Theoretical calculations indicate, however, that the V_O donor level is deeper than 2 eV from the conduction band [28]. It should also be noted that emission from BL was suppressed in Si-doped β-Ga_2O_3 compared to UVL, as seen from previously reported studies [42].

AIP Publishing

ACCEPTED MANUSCRIPT

This is the author's peer reviewed, accepted manuscript. However, the online version of record will be different from this version once it has been copyedited and typeset.
PLEASE CITE THIS ARTICLE AS DOI:10.1063/5.0073692

AIP Advances

Fig. 1d, left and right, show the normalized spectra for the reference, proton- and alpha-particle-irradiated samples at 4.5 K and 310 K, respectively. Deep Level Transient Spectroscopy (DLTS) studies on HVPE grown Si-doped β-Ga2O3 with similar concentration irradiated with 10 MeV proton-irradiated and 18 MeV alpha-particle-irradiated Si-doped HVPE β-Ga_2O_3 identified new trap-levels and change in the concentration of existing levels [20, 51]. 10 MeV proton irradiation showed a new trap-level (E_4) at E_c-1.2 eV, associated with native defect complexes [20]. Additionally, E_4 and H_3 (E_v+1.2 eV) levels appeared in high densities after irradiation. 18 MeV alpha-particle-irradiation introduced a hole trap at E_v+1.4 eV, associated with complexes formed by V_{Ga} with shallow donors and V_{Ga} with hydrogen, an electron trap E_5 (E_c-1.35 eV), and there was an increase in the concentration of existing trap levels [51, 52]. As seen in Fig. 1d, the shape of the CL spectra remains virtually unchanged for irradiated and reference samples. Therefore, it could be inferred that the new radiation induced E_4 and E_v+1.4 eV traps do not participate in radiative recombination within the current temperature regime of observation. The increase in the concentration of primary trap levels and their associated complexes are responsible for the change in the CL emission intensity and activation energies associated with the thermal quenching process, as discussed below. Fig 2 shows the energy levels changes by proton and alpha-particle irradiation after ref. [20, 51].

Fig. 3a depicts the temperature dependence of intensities for UVL', UVL and BL. UVL' and UVL undergo much stronger thermal quenching with increase in temperature compared to BL, as seen from the relative change in the intensity over the entire temperature range. The temperature-dependent integrated CL intensity of UVL' and UVL was analyzed with the following analytic equation:

$$I(T) = I_0/(1 + A_1 e^{-E_{A1}/k_B T} + A_2 e^{-E_{A2}/k_B T}) \quad (1)$$

AIP Publishing

ACCEPTED MANUSCRIPT

This is the author's peer reviewed, accepted manuscript. However, the online version of record will be different from this version once it has been copyedited and typeset.
PLEASE CITE THIS ARTICLE AS DOI:10.1063/5.0073692

AIP Advances

Here, I_0 is the integrated CL intensity at 0 K; A_i and E_{Ai} are amplitude and thermal activation energy of the temperature activated processes; k_B is the Boltzmann constant; T is the temperature. The fit using Eq. (1) for UVL' and UVL temperature dependence is shown in Fig. 3b and 3c. E_{A1} and E_{A2} for reference, proton- and alpha-irradiated samples are summarized in Table 1. Both E_{A1} and E_{A2} are comparable in the case of reference and proton-irradiated samples and decrease substantially for alpha-irradiated samples. E_{A1} could be attributed to the ionization of shallow Si donors that have ionization energy ~ 31 is meV [53]. Calculated values of E_{A2} are comparable for UVL' and UVL and, therefore, could be attributed to a single non-radiative recombination center (NRC) responsible for the thermal quenching [40, 41]. E_{A2} is close to the previously reported activation energy measured for UVL emission by Onuma *et al.* [40]. Fe^{3+}/Fe^{2+} was suggested as an efficient non-radiative recombination channel in as-grown EFG Si-doped β-Ga_2O_3 [41], but it should be noted that the concentration of transition metal impurities is roughly 2 orders of magnitude lower in HVPE Si-doped β-Ga_2O_3 [20, 52]. In a different report, E_{A2} was attributed to a combination of Auger recombination and migration through tunnelling of STHs to a V_{Ga}^{-3} centers forming V_{Ga}^{-2} acceptors [31, 54].

Kananen *et al.* [31] found that STHs are only stable below 90 K. Above 110 K, 96 % of the STHs decay and simultaneously, the V_{Ga}^{-2}concentration increases with an activation energy of ~ 190 meV, much smaller than the hole self-trapping energy of 0.53 eV [29]. This process could be a likely explanation of the relatively low thermal quenching observed for the BL band compared to UVL' and UVL bands. With the activation of NRC as a competing parallel recombination channel, all three emission bands experience quenching. STH tunneling causes increase in the concentration of V_{Ga}^{-2} centers, which act as acceptors in the recombination process responsible for

AIP Publishing

ACCEPTED MANUSCRIPT

This is the author's peer reviewed, accepted manuscript. However, the online version of record will be different from this version once it has been copyedited and typeset.
PLEASE CITE THIS ARTICLE AS DOI:10.1063/5.0073692

AIP Advances

BL emission. Therefore, despite the activation of NRC, BL intensity reduces only by ~ 30% for reference sample (~ 35% and 45% for proton- and alpha-particle-irradiated samples, respectively).

A raw TRCL streak image of the reference sample is show in Fig. 3d (inset, top). The integrated decay for the UVL band (Fig. 3d top inset, shown between the dotted lines) is shown in Fig. 3d (inset, bottom). The TRCL streak is fitted with a single exponential decay

$$A(t) = A_0 \exp(-t/\tau) + C. \quad (2)$$

Here, A_0 is a constant, t is excitation delay, τ is the TRCL lifetime and C is a constant associated with slow decay in the luminescence. The temperature dependence of lifetime for the reference, proton and alpha-irradiated samples is shown in Fig. 3d. τ reduces roughly by factor of 3 with increasing temperature for both irradiated and reference samples (additional detains in ref. [17]). To directly verify lifetime quenching by the thermal activation of NRC, the approach laid out in refs. [55, 56] was used. Temperature dependence of τ is given by following equation:

$$\tau(T) = \tau_0/(1 + A_\tau e^{-E_{A\tau}/k_B T}) \quad (3)$$

Here, τ is the measured lifetime; τ_0 is lifetime before the advent of thermal quenching; A_τ is a constant that depends on τ_0, internal quantum efficiency of the luminescence band, and effective density of states in the valence band. Fitting the temperature dependence of τ from Fig. 3d yields $E_{A\tau}$ as 73.7 meV for the reference sample, which matches well with the value of E_{A2} calculated in the thermal quenching analysis above. $E_{A\tau}$ for proton- and alpha-particle-irradiated samples was 77.8 and 80.8 meV, respectively. It should be noted that the lifetime mentioned above is calculated from the intensity decay of the entire integrated luminescence spectrum and not isolated bands. Therefore, the method for calculation of the NRC thermal activation energy is approximate and could be a likely reason for the difference between activation energy obtained from Eqn. (3) and from thermal quenching of UVL' and UVL luminescence, as seen in Table 1.

AIP Publishing

ACCEPTED MANUSCRIPT

This is the author's peer reviewed, accepted manuscript. However, the online version of record will be different from this version once it has been copyedited and typeset.
PLEASE CITE THIS ARTICLE AS DOI:10.1063/5.0073692

AIP Advances

Irradiation caused a decrease in both thermal activation energies E_{A1} and E_{A2}, pertaining to shallow donors and activation of deep NRCs, for both UVL' and UVL bands. Lowering of the shallow donor ionization energy (E_{A1}) due to high-energy electron, proton- and alpha-particle-irradiation was observed in EBIC measurements [17, 20, 36]. Decrease in E_{A1} indicates the shallow donor level moving closer to the conduction band minima, facilitating transport of electrons to conduction band with lower activation energy. Even though E_{A1} reduces, due to the introduction of new defects and increase in the density of existing defects, the total number of carriers is lower compared to the unirradiated sample, which is reflected by the carrier removal rates. In the DLTS measurements [20, 51], the carrier removal rate for the irradiated samples could not be completely explained by the radiation-induced increase in the concentration of primary traps alone, as shallow donors and radiation-induced trap levels form neutral complexes and the nature of these trap levels is not exactly known [51]. The temperature dependent CL measurements from this work suggest that the defect complexes do not participate in the radiative recombination process in the temperature range of the measurements (4.5 K - 310 K). The origin of the NRC and the role of the neutral complex in the supplementation of this recombination pathway (reduction of E_{A2}) will be the focus of a future study.

In summary, temperature-dependent cathodoluminescence and time-resolved cathodoluminescence measurements were employed to understand the luminescence from HVPE Si-doped β-Ga_2O_3, before and after irradiation with 10 MeV protons and 18 MeV alpha-particles. No new luminescence bands were detected in the CL spectra of the irradiated samples. Moreover, the peak location remained the same for all three samples at a given temperature, indicating that the introduced radiation-induced new trap-levels did not create new channels facilitating radiative recombination. Two activation energies were extracted from the thermal quenching of UVL and

AIP Publishing

ACCEPTED MANUSCRIPT

This is the author's peer reviewed, accepted manuscript. However, the online version of record will be different from this version once it has been copyedited and typeset.
PLEASE CITE THIS ARTICLE AS DOI:10.1063/5.0073692

AIP Advances

UVL' band, pertaining to ionization of shallow donors and a thermally-activated non-radiative recombination channel. Additionally, reduction in activation energies associated with shallow donors and non-radiative recombination centers was observed due to radiation damage.

Data Availability Statement

All data that support the findings of this study are included within the article.

Acknowledgements

Research at UCF was supported in part by NSF (ECCS awards 1802208 and 2127916). Research at UCF and Tel Aviv University was supported in part by US-Israel BSF (2018010) and NATO (G5748). The work at UF was performed as part of Interaction of Ionizing Radiation with Matter University Research Alliance (IIRM-URA), sponsored by the Department of the Defense, Defense Threat Reduction Agency under award HDTRA1-20-2-0002 (Jacob Calkins). The content of the information does not necessarily reflect the position or the policy of the federal government, and no official endorsement should be inferred. The work at UF was also supported by NSF DMR 1856662 (James Edgar).

Conflict of interest declaration

The authors have no conflicts to disclose.

AIP Publishing

ACCEPTED MANUSCRIPT

This is the author's peer reviewed, accepted manuscript. However, the online version of record will be different from this version once it has been copyedited and typeset.
PLEASE CITE THIS ARTICLE AS DOI:10.1063/5.0073692

AIP Advances

References

1. S.J. Pearton, J. Yang, P.H. Cary, F. Ren, J. Kim, M.J. Tadjer, and M.A. Mastro, Appl. Phys. Rev. **5**, 011301 (2018).
2. J.H. Park, D.Y. Kim, E.F. Schubert, J. Cho, and J.K. Kim, ACS Energy Lett. **3**, 655 (2018).
3. M. Higashiwaki and G.H. Jessen, Appl. Phys. Lett. **112**, 060401 (2018).
4. J. Yang, S. Ahn, F. Ren, S.J. Pearton, S. Jang, and A. Kuramata, IEEE Electr. Device L. **38**, 906 (2017).
5. H. von Wenckstern, Adv. Electron. Mater. **3**, 1600350 (2017).
6. M.A. Mastro, A. Kuramata, J. Calkins, J. Kim, F. Ren, and S.J. Pearton, ECS J. Solid State Sci. Technol. **6**, P356 (2017).
7. H. Masataka, K. Akito, M. Hisashi, and K. Yoshinao, J. Phys. D **50**, 333002 (2017).
8. K. Konishi, K. Goto, H. Murakami, Y. Kumagai, A. Kuramata, S. Yamakoshi, and M. Higashiwaki, Appl. Phys. Lett. **110**, 103506 (2017).
9. E. Chikoidze, A. Fellous, A. Perez-Tomas, G. Sauthier, T. Tchelidze, C. Ton-That, T.T. Huynh, M. Phillips, S. Russell, M. Jennings, B. Berini, F. Jomard, and Y. Dumont, Mater. Today Phys. **3**, 118 (2017).
10. S. Ahn, F. Ren, S. Oh, Y. Jung, J. Kim, M.A. Mastro, J.K. Hite, C.R. Eddy, and S.J. Pearton, Journal of Vacuum Science & Technology B, Nanotechnology and Microelectronics: Materials, Processing, Measurement, and Phenomena **34**, 041207 (2016).
11. S. Oh, Y. Jung, M. A. Mastro, J. K. Hite, C. R. Eddy Jr., and J. Kim, Opt. Express **23**, 28300 (2015).

AIP Publishing

ACCEPTED MANUSCRIPT
AIP Advances
This is the author's peer reviewed, accepted manuscript. However, the online version of record will be different from this version once it has been copyedited and typeset.
PLEASE CITE THIS ARTICLE AS DOI:10.1063/5.0073692
AIP Publishing

12. J. Kim, S.J. Pearton, C. Fares, J. Yang, F. Ren, S. Kim, and A.Y. Polyakov, J. Mater. Chem. C **7**, 10 (2019).

13. B. Liu, M. Gu, and X. Liu, Appl. Phys. Lett. **91**, 172102 (2007).

14. H. He, R. Orlando, M.A. Blanco, R. Pandey, E. Amzallag, I. Baraille, and M. Rérat, Phys. Rev. B **74**, 195123 (2006).

15. M.H. Wong, A. Takeyama, T. Makino, T. Ohshima, K. Sasaki, A. Kuramata, S. Yamakoshi, and M. Higashiwaki, Appl. Phys. Lett. **112**, 023503 (2018).

16. G. Yang, S. Jang, F. Ren, S.J. Pearton, and J. Kim, ACS Appl. Mater. Interfaces **9**, 40471 (2017).

17. S. Modak, L. Chernyak, A. Schulte, M. Xian, F. Ren, S.J. Pearton, I. Lubomirsky, A. Ruzin, S.S. Kosolobov, and V.P. Drachev, Appl. Phys. Lett. **118**, 202105 (2021).

18. S. Modak, L. Chernyak, S. Khodorov, I. Lubomirsky, A. Ruzin, M. Xian, F. Ren, and S.J. Pearton, ECS J. Solid State Sci. Technol. **9**, 045018 (2020).

19. J. Yang, Z. Chen, F. Ren, S.J. Pearton, G. Yang, J. Kim, J. Lee, E. Flitsiyan, L. Chernyak, and A. Kuramata, J. Vac. Sci. Technol. B Nanotechnol. Microelectron. **36**, 011206 (2018).

20. A.Y. Polyakov, N.B. Smirnov, I.V. Shchemerov, E.B. Yakimov, J. Yang, F. Ren, G. Yang, J. Kim, A. Kuramata, and S.J. Pearton, Appl. Phys. Lett. **112**, 032107 (2018).

21. A.Y. Polyakov, N.B. Smirnov, I.V. Shchemerov, S.J. Pearton, F. Ren, A.V. Chernykh, P.B. Lagov, and T.V. Kulevoy, APL Mater. **6**, 096102 (2018).

22. S. Ahn, Y.-H. Lin, F. Ren, S. Oh, Y. Jung, G. Yang, J. Kim, M.A. Mastro, J.K. Hite, C.R. Eddy, and S.J. Pearton, J. Vac. Sci. Technol. B Nanotechnol. Microelectron. **34**, 041213 (2016).

ACCEPTED MANUSCRIPT

This is the author's peer reviewed, accepted manuscript. However, the online version of record will be different from this version once it has been copyedited and typeset.
PLEASE CITE THIS ARTICLE AS DOI:10.1063/5.0073692

AIP Advances

23. L.N. Cojocaru, Radiation Effects **21**, 157 (2006).
24. S. Modak, L. Chernyak, S. Khodorov, I. Lubomirsky, J. Yang, F. Ren, and S.J. Pearton, ECS J. Solid State Sci. Technol. **8**, Q3050 (2019).
25. J. Yang, C. Fares, Y. Guan, F. Ren, S.J. Pearton, J. Bae, J. Kim, and A. Kuramata, J. Vac. Sci. Technol. B **36**, 031205 (2018).
26. T. Harwig, F. Kellendonk, J. Solid State Chem. **24**, 255 (1978).
27. G. Blasse and A. Bril, J. Phys. Chem. Solids **31**, 707 (1970).
28. Q.D. Ho, T. Frauenheim, and P. Deák, Phys. Rev. B **97**, 115163 (2018).
29. J.B. Varley, A. Janotti, C. Franchini, and C.G. Van de Walle, Phys. Rev. B **85**, 4 (2012).
30. S. Yamaoka and M. Nakayama, Phys. Status Solidi C **13**, 93 (2016).
31. B.E. Kananen, N.C. Giles, L.E. Halliburton, G.K. Foundos, K.B. Chang, and K.T. Stevens, J. Appl. Phys. **122**, 215703 (2017).
32. S. Modak, J. Lee, L. Chernyak, J. Yang, F. Ren, S.J. Pearton, S. Khodorov, and I. Lubomirsky, AIP Adv. **9**, 015127 (2019).
33. E.B. Yakimov, Crystallogr. Rep. **66**, 581 (2021).
34. E.B. Yakimov, A.Y. Polyakov, N.B. Smirnov, I.V. Shchemerov, P.S. Vergeles, E.E. Yakimov, A.V. Chernykh, M. Xian, F. Ren, and S.J. Pearton, J. Phys. D **53**, 495108 (2020).
35. E.B. Yakimov, A.Y. Polyakov, N.B. Smirnov, I.V. Shchemerov, J. Yang, F. Ren, G. Yang, J. Kim, and S.J. Pearton, J. Appl. Phys. **123**, 185704 (2018).
36. J. Lee, E. Flitsiyan, L. Chernyak, J. Yang, F. Ren, S.J. Pearton, B. Meyler, and Y.J. Salzman, Appl. Phys. Lett. **112**, 082104 (2018).

AIP Publishing

ACCEPTED MANUSCRIPT
AIP Advances
This is the author's peer reviewed, accepted manuscript. However, the online version of record will be different from this version once it has been copyedited and typeset.
PLEASE CITE THIS ARTICLE AS DOI:10.1063/5.0073692
AIP Publishing

37. J. Lapp, D. Thapa, J. Huso, A. Canul, M. McCluskey, and L. Bergman. Bull. Am. Phys. Soc. (2020).

38. S. Marcinkevičius and J.S. Speck, Appl. Phys. Lett. **116**, 132101 (2020).

39. S. Yamaoka, Y. Furukawa, and M. Nakayama, Phys. Rev. B **95**, 094304 (2017).

40. T. Onuma, Y. Nakata, K. Sasaki, T. Masui, T. Yamaguchi, T. Honda, A. Kuramata, S. Yamakoshi, and M. Higashiwaki, J. Appl. Phys. **124**, 075103 (2018).

41. T.T. Huynh, L.L.C. Lem, A. Kuramata, M.R. Phillips, and C. Ton-That, Phys. Rev. Mater. **2**, 105203 (2018).

42. T. Onuma, S. Fujioka, T. Yamaguchi, M. Higashiwaki, K. Sasaki, T. Masui, and T. Honda, Appl. Phys. Lett. **103**, 041910 (2013).

43. L. Binet and D. Gourier, J. Phys. Chem. Solid **59**, 1241 (1998).

44. Y.K. Frodason, K.M. Johansen, L. Vines, and J.B. Varley, J. Appl. Phys. **127**, 075701 (2020).

45. R.T. Williams and K.S. Song, J. Phys. Chem. Solids **51**, 679 (1990).

46. P. Deák, Q. Duy Ho, F. Seemann, B. Aradi, M. Lorke, and T. Frauenheim, Phys. Rev. B **95**, 075208 (2017).

47. M. Yamaga, T. Ishikawa, M. Yoshida, T. Hasegawa, E.G. Villora, and K. Shimamura, Phys. Status Solidi C **8**, 2621 (2011).

48. S. Yamaoka, Y. Mikuni, and M. Nakayama, J. Phys. Conf. Ser. **1220**, 012030 (2019).

49. K. Shimamura, E.G. Víllora, T. Ujiie, and K. Aoki, Appl. Phys. Lett. **92**, 201914 (2008).

50. Y. Wang, P.T. Dickens, J.B. Varley, X. Ni, E. Lotubai, S. Sprawls, F. Liu, V. Lordi, S. Krishnamoorthy, S. Blair, K.G. Lynn, M. Scarpulla, and B. Sensale-Rodriguez, Sci. Rep. **8**, 18075 (2018).

ACCEPTED MANUSCRIPT

This is the author's peer reviewed, accepted manuscript. However, the online version of record will be different from this version once it has been copyedited and typeset.
PLEASE CITE THIS ARTICLE AS DOI:10.1063/5.0073692

AIP Advances

51. A.Y. Polyakov, N.B. Smirnov, I.V. Shchemerov, E.B. Yakimov, S.J. Pearton, C. Fares, J. Yang, F. Ren, J. Kim, P.B. Lagov, V.S. Stolbunov, and A. Kochkova, Appl. Phys. Lett. **113**, 092102 (2018).

52. Z. Wang, X. Chen, F.-F. Ren, S. Gu, and J. Ye, J. Phys. D **54**, 043002 (2020).

53. A.T. Neal, S. Mou, S. Rafique, H. Zhao, E. Ahmadi, J.S. Speck, K.T. Stevens, J.D. Blevins, D.B. Thomson, N. Moser, K.D. Chabak, and G.H. Jessen, Appl. Phys. Lett. **113**, 062101 (2018).

54. H. Tang, N. He, Z. Zhu, M. Gu, B. Liu, J. Xu, M. Xu, L. Chen, J. Liu, and X. Ouyang, Appl. Phys. Lett. **115**, 071904 (2019).

55. M.A. Reshchikov, Phys. Status Solidi A **218**, 2000101 (2020).

56. M.A. Reshchikov, J. Appl. Phys. **115**, 103503 (2014).

AIP Publishing

ACCEPTED MANUSCRIPT
AIP Advances
This is the author's peer reviewed, accepted manuscript. However, the online version of record will be different from this version once it has been copyedited and typeset.
PLEASE CITE THIS ARTICLE AS DOI:10.1063/5.0073692
AIP Publishing

Table 1: The activation energies (in meV) E_{A1} and E_{A2} calculated for UVL' and UVL bands, for reference, proton- and alpha-irradiated samples respectively.

	UVL'		UVL	
	E_{A1} (meV)	E_{A2} (meV)	E_{A1} (meV)	E_{A2} (meV)
Reference	31.8	75.3	34.1	74.9
Proton	32.3	74.6	34.7	70.4
Alpha	26.1	70.9	29.2	63.4

ACCEPTED MANUSCRIPT

This is the author's peer reviewed, accepted manuscript. However, the online version of record will be different from this version once it has been copyedited and typeset.
PLEASE CITE THIS ARTICLE AS DOI:10.1063/5.0073692

AIP Advances

Figure Captions

Figure 1: (a) Normalized CL emission spectrum for temperatures ranging from 4.5 to 310 K. **(b, c)** Gaussian decomposition of the CL spectra into three constituent peaks - UVL' (3.63 eV), UVL (3.3 eV), and BL (2.96 eV), for 4.5 K and 310 K respectively. **(d)** Normalized spectra for reference, proton- and alpha-particle-irradiated samples at 4.5 K (left) and 310 K (right).

Figure 2: Energy level diagram (not to scale) of the trap levels in HVPE grown Si-doped β-Ga_2O_3 irradiated with 10 MeV protons and 18 MeV alpha-particles obtained from DLTS measurements (after refs. [20, 51]). Proton irradiation introduces new level (E_4) and significantly increases the concentration of E_c-2.3 eV, E_4 and H_3. Alpha particle irradiation introduces a new levels at E_v+1.4 eV and E_5 (E_c-1.35 eV) and additionally, increased the concentration of existing trap levels (E_2^*-E_4 and H_3).

Figure 3: (a) Temperature dependence of UVL', UVL and BL bands. **(b, c)** Fit of UVL' and UVL data with Eq. (1) for estimation of the thermal activation energies. The plots for reference, proton- and alpha-particle-irradiated samples are shifted vertically for visual clarity. **(d)** Temperature dependence of TRCL lifetime.

AIP Publishing

ACCEPTED MANUSCRIPT

AIP Advances

This is the author's peer reviewed, accepted manuscript. However, the online version of record will be different from this version once it has been copyedited and typeset.
PLEASE CITE THIS ARTICLE AS DOI:10.1063/5.0073692

Figure 1

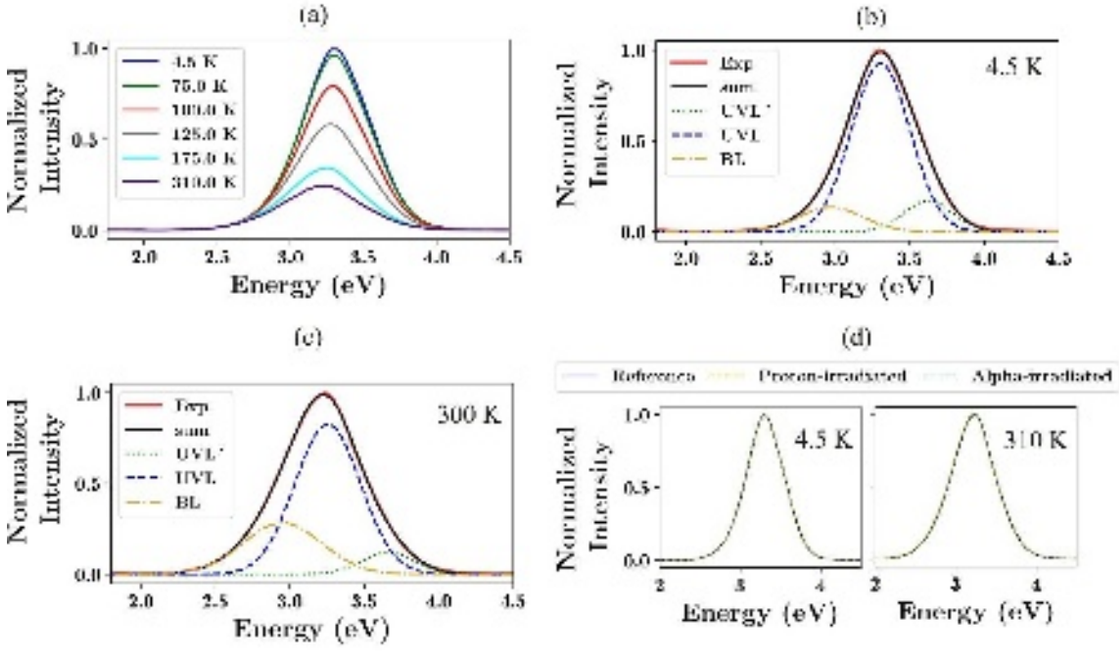

ACCEPTED MANUSCRIPT
AIP Advances
This is the author's peer reviewed, accepted manuscript. However, the online version of record will be different from this version once it has been copyedited and typeset.
PLEASE CITE THIS ARTICLE AS DOI:10.1063/5.0073692
AIP Publishing

Figure 2

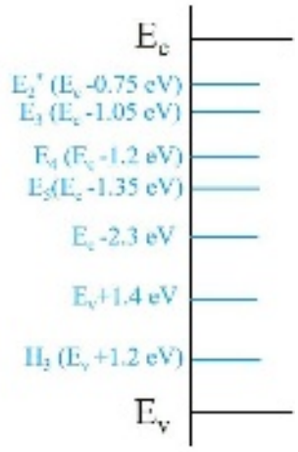

ACCEPTED MANUSCRIPT

AIP Advances

This is the author's peer reviewed, accepted manuscript. However, the online version of record will be different from this version once it has been copyedited and typeset.
PLEASE CITE THIS ARTICLE AS DOI:10.1063/5.0073692

Figure 3

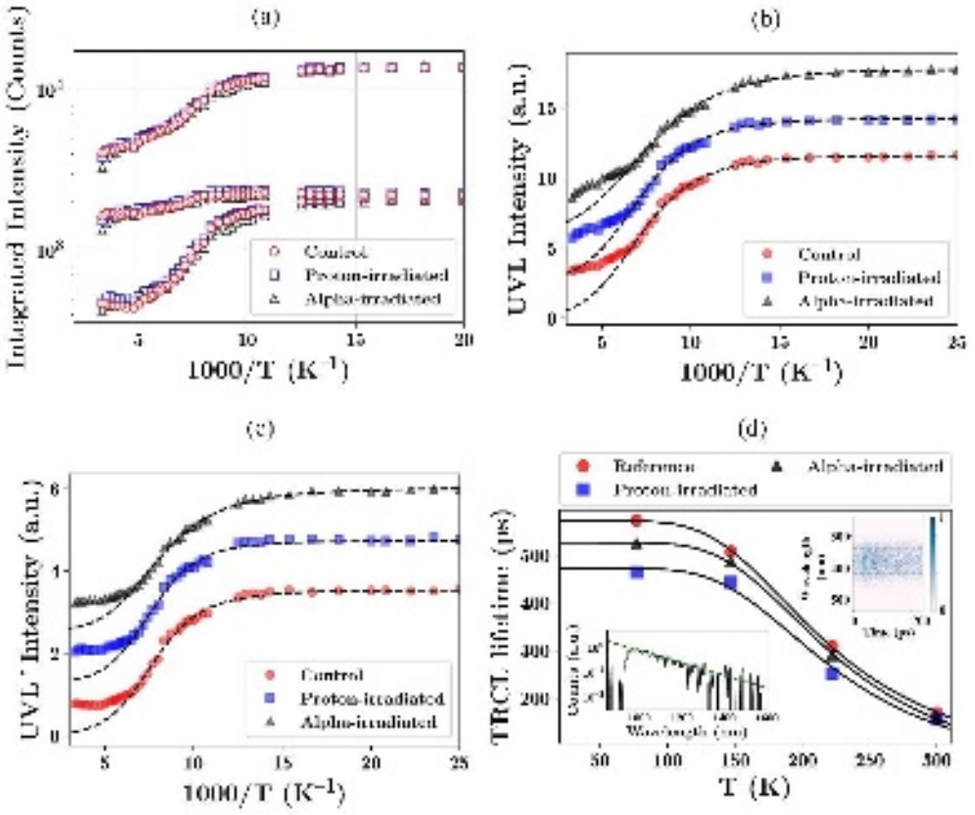

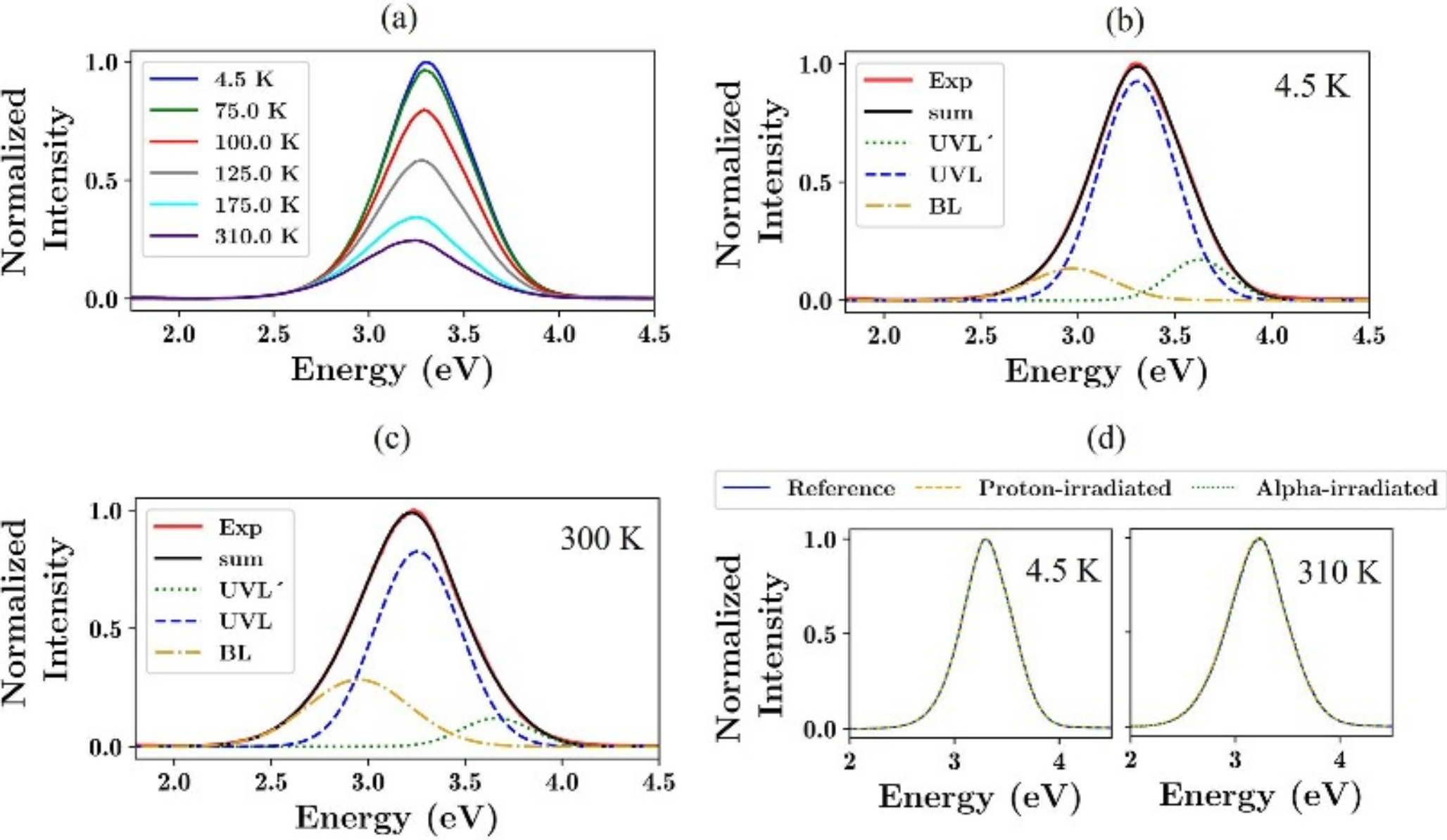
(a)
Normalized Intensity
4.5 K
75.0 K
100.0 K
125.0 K
175.0 K
310.0 K
Energy (eV)
(b)
4.5 K
Exp
sum
UVL´
UVL
BL
Energy (eV)
(c)
300 K
Exp
sum
UVL´
UVL
BL
Energy (eV)
(d)
Reference
Proton-irradiated
Alpha-irradiated
4.5 K
310 K
Energy (eV)
Energy (eV)


E_c
E_2^* (E_c -0.75 eV)
E_1 (E_c -1.05 eV)
E_x (E_c -1.2 eV)
E_d(E_c -1.35 eV)
E_c -2.3 eV
E_t -1.4 eV
H_3 (E_v +1.2 eV)
E_v

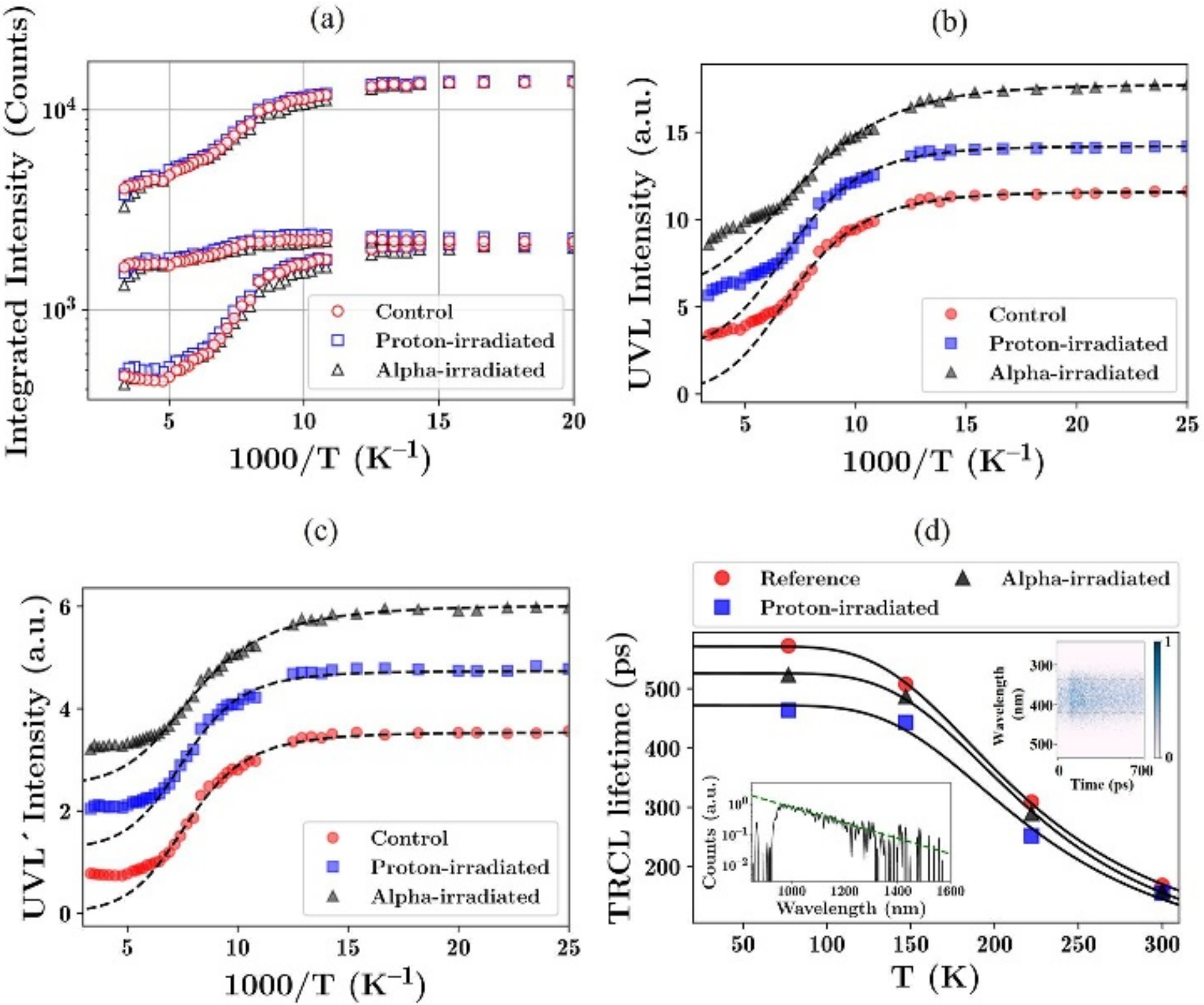
(a)
Integrated Intensity (Counts)
10^4
10^3
5
10
15
20
1000/T (K^{-1})
Control
Proton-irradiated
Alpha-irradiated
(b)
UVL Intensity (a.u.)
0
5
10
15
5
10
15
20
25
1000/T (K^{-1})
Control
Proton-irradiated
Alpha-irradiated
(c)
UVL´ Intensity (a.u.)
0
2
4
6
5
10
15
20
25
1000/T (K^{-1})
Control
Proton-irradiated
Alpha-irradiated
(d)
Reference
Proton-irradiated
Alpha-irradiated
TRCL lifetime (ps)
200
300
400
500
50
100
150
200
250
300
T (K)
Wavelength (nm)
300
400
500
0
700
Time (ps)
1
0
Counts (a.u.)
10^0
10^{-1}
10^{-2}
1000
1200
1400
1600
Wavelength (nm)